

wind stress curl changes is a delayed process and would retard the existing cyclonic circulation. We would expect this influence to manifest itself with large reversals in PC1 of the geostrophic velocity like the variations in the curl PC1 or NAO with a 3- to 5-year delay. Figure 5C shows that there are peaks in geostrophic velocity PC1 with such a delay, but they are small relative to the overwhelming background trend.

Property 3 of the continuous weakening of the subpolar air-sea heat loss is consistent with the observations that deep convective conditions in the Labrador Sea have been absent since the early 1990s. Although changes in advection of heat can have as much as 50% effect on the subpolar heat storage changes (10), the local heat flux changes are still important, particularly in forcing deep convection. Because deep convection maintains a cold core around which lighter water masses circulate, cessation of deep convection would lead to a decaying baroclinic gyre. This decaying cold core of the Labrador Gyre from 1992 to 2002 is observable in the dynamic height increase (using WOCE section AR7/W), which is about 6 cm relative to 1000db (Fig. 1A) (fig. S3) and comparable with the altimeter SSH change. The strong height gradient associated with boundary currents is important to inferences of circulation; this is seen in the hydrography (fig. S3). Evidence from the hydrographic data together with the 1990s heat flux trend is supportive of a connection between convective forcing and the observed decline in the gyre strength. It might not have been the case if wind-driven barotropic circulation or overflow-driven circulation variability were dominant causes.

Conclusions. Altimetric geostrophic circulation observations and supporting deep-sea current-meter observations suggest significant changes over the last two decades, with increasing SSH and weakening subpolar gyre circulation in the 1990s. By comparing the dynamic consequences of three mechanisms, buoyancy forcing and barotropic and baroclinic response to local wind stress curl, we find that the gyre weakening in the 1990s is not attributable to local wind stress changes associated with NAO. The weakening-gyre scenario of the 1990s parallels the warming in the central subpolar gyre, which is the well-observed relaxation of the water column following the intense winter convection period of 1989–1994. The lack of deep convection is the oceanic response to the local buoyancy forcing, which has mimicked low-NAO heat fluxes even though the index itself has reversed itself twice during the 1990s.

Because we lack SSH data before 1978, we cannot determine whether the 1990s slowing gyre is a part of a decadal cycle or the beginning of a longer term trend. Because Labrador Sea processes are intimately linked to the meridional overturning circulation, involving both intermediate-depth and deep waters, these observations of rapid climatic

changes over one decade may merit some concern for the future state of the MOC. Continuation of the altimeter missions will allow us to follow the evolution of this subpolar signal and its influence on the North Atlantic. Field observations of the subsurface oceanic circulation, hydrography, and ice cover (28) will be of great importance in establishing the origin of these climate shifts.

References and Notes

1. J. W. Hurrell, *Science* **269**, 676 (1995).
2. R. R. Dickson *et al.*, *Nature* **416**, 832 (2002).
3. J. R. N. Lazier *et al.*, *Deep-Sea Res.* **49**, 1819 (2002).
4. C. Deser, M. L. Blackmon, *J. Clim.* **6**, 1743 (1993).
5. G. Reverdin, D. Cayan, Y. Kushnir, *J. Geophys. Res.* **102**, 8505 (1997).
6. I. M. Belkin, S. Levitus, J. Antonov, S.-A. Malmberg, *Prog. Oceanogr.* **41**, 1 (1998).
7. R. G. Curry, M. S. McCartney, *J. Phys. Oceanogr.* **31**, 3374 (2001).
8. R. R. Dickson, J. Meincke, S.-A. Malmberg, A. J. Lee, *Prog. Oceanogr.* **20**, 103 (1988).
9. G. Han, C. L. Tang, *J. Phys. Oceanogr.* **31**, 199 (2001).
10. N. Verbrugge, G. Reverdin, *J. Phys. Oceanogr.* **33**, 964 (2003).
11. M. K. Flatau, L. Talley, P. P. Niiler, *J. Clim.* **16**, 2355 (2003).
12. B. Hansen, W. Turrell, S. Osterhus, *Nature* **411**, 927 (2001).
13. R. S. Pickart *et al.*, *Nature* **424**, 152 (2003).
14. A. S. Bower *et al.*, *Nature* **419**, 603 (2002).
15. M. A. White, K. J. Heywood, *J. Geophys. Res.* **100**, 24931 (1995).
16. J. Cuny, P. B. Rhines, P. P. Niiler, S. Bacon, *J. Phys. Oceanogr.* **32**, 627 (2002).
17. D. M. Fratantoni, *J. Geophys. Res.* **106**, C1022067 (2001).
18. The RAFOS floats (14) highlight meridional pathways at depths ranging from near-surface to 1500 m. White and Heywood (15) argued from early altimeter data that changing winds can shift the site of northward flow; Cuny *et al.* (16) and Fratantoni (17) compared surface drifter data with satellite altim-

- etry, yet data density was not sufficient to show significant changes between the 1990s and 1980s.
19. S. Häkkinen, *J. Geophys. Res.* **106**, 13837 (2001).
 20. C. Eden, J. Willebrand, *J. Clim.* **14**, 2266 (2001).
 21. R. Döscher, C. W. Böning, P. Herrmann, *J. Phys. Oceanogr.* **24**, 2306 (1994).
 22. W. M. Smethie, R. A. Fine, *Deep-Sea Res.* **48**, 189 (2001).
 23. Mapping the distribution of natural and human-made trace chemicals is an "accurate" way to view the MOC [see, e.g., (22)].
 24. The "normal" heat flux pattern corresponding to NAO has the Labrador Sea out of phase with the Greenland-Norwegian Sea (29), but the eastward migration of the Icelandic Low has altered this relationship since 1995.
 25. P. B. Rhines, *J. Fluid Mech.* **37**, 161 (1969).
 26. R. J. Greatbatch, A. D. Goulding, *J. Phys. Oceanogr.* **19**, 572 (1989).
 27. Wind-driven currents are set up by propagation of topographic Rossby waves along f/h (Coriolis frequency/total depth) contours, eventually approximating a topographic-Sverdrup balance. This produces over a matter of a few weeks a single anticyclonic gyre, or "intergyre," centered at 50°N latitude, at the boundary between subpolar and subtropical gyres. The Mid-Atlantic Ridge dominates this f/h waveguide (25, 26).
 28. The Arctic-SubArctic Flux Program (ASOF) (<http://asof.npolar.no>) is an observational campaign bridging programs such as SEARCH and CLIVAR.
 29. R. R. Dickson *et al.*, *Prog. Oceanogr.* **38**, 241 (1996).
 30. Supported by the NASA Physical Oceanography Program (S.H.) and by the NOAA Arctic Research Office, Vetlesen Foundation, and the NSF Office of Polar Programs (P.B.R.). The Office of Naval Research and Bedford Institute of Oceanography supported the current-meter measurements. We thank J. R. N. Lazier, I. Yashayev, and J. Cuny for help with the subsurface ocean data, and D. Worthen for assistance with graphics.

Supporting Online Material

www.sciencemag.org/cgi/content/full/304/5670/555/DC1
Figs. S1 to S3

19 December 2003; accepted 20 March 2004

Synfire Chains and Cortical Songs: Temporal Modules of Cortical Activity

Yuji Ikegaya,^{1*} Gloster Aaron,^{1*} Rosa Cossart,¹
Dmitriy Aronov,¹ Ilan Lampl,² David Ferster,² Rafael Yuste^{1†}

How can neural activity propagate through cortical networks built with weak, stochastic synapses? We find precise repetitions of spontaneous patterns of synaptic inputs in neocortical neurons *in vivo* and *in vitro*. These patterns repeat after minutes, maintaining millisecond accuracy. Calcium imaging of slices reveals reactivation of sequences of cells during the occurrence of repeated intracellular synaptic patterns. The spontaneous activity drifts with time, engaging different cells. Sequences of active neurons have distinct spatial structures and are repeated in the same order over tens of seconds, revealing modular temporal dynamics. Higher order sequences are replayed with compressed timing.

The essence of cortical function is the propagation and transformation of neuronal activity by the cortical circuit (1). How activity can propagate through a network composed of weak, stochastic, and depressing synapses is, however, poorly understood (2–4). It has been proposed that sequences of synchronous activity ("synfire chains") propagate through

the cortical circuit with high temporal fidelity (5, 6). Synchronous summation of excitatory postsynaptic potentials (EPSPs) could ensure postsynaptic firing and the nonlinear gain caused by the spike threshold could preserve temporal fidelity, so reactivations of the same chain would result in exact repetitions of precise firing patterns (7). Repetitions of

temporally precise firing sequences of spikes have been reported (7, 8), although their existence is controversial (9).

If synfire chains, or precisely timed repetitions of spike sequences, exist in cortical activity, the reactivation of the same spatio-temporal pattern of activity should produce, as its postsynaptic signature, repetitions of patterns of synaptic activity in intracellular recordings from single neurons in the network. If a recorded neuron receives connections from cells located at different points in a chain, it will receive temporally stereotypical patterns of excitatory and inhibitory postsynaptic potentials (EPSPs and IPSPs) as the chain repeats its pattern of spikes. We searched systematically for repeated patterns of spontaneous synaptic inputs in pyramidal

neurons, using intracellular recordings from slices of mouse primary visual cortex or from intact cat primary visual cortex *in vivo* (10).

Precisely repeating motifs of spontaneous synaptic activity in slices. To detect repetitions of spontaneous activity, we calculated the covariance between any two segments of an intracellular recording (11), with low- (1 s; low resolution index, LRI) and high- (20 ms; high resolution index, HRI) resolution windows of analysis (fig. S1). The low-resolution window was used to identify regions of the traces with potential repeats; these regions were then scanned at high resolution. In 20 voltage-clamp recordings of spontaneous activity from slices (8 min long), we encountered repetitions of sequences of spontaneous activity with high HRI values and marked similarity in the patterns of positive and negative deflections in the membrane current (“motifs”) (Fig. 1). Because recordings were taken at -70 mV, most repeated patterns were composed of EPSCs (5 to 20 pA). A total of 17,055 motifs passing minimum thresholds for HRI were found in 18 out of 20 cells (Fig. 1A), and different statistical analyses confirmed that they were not due to chance (fig.

S2, A to C). Moreover, motifs above chance level were not found in recordings of miniature EPSCs in slices under $1 \mu\text{M}$ tetrodotoxin (fig. S2, D and E) [control artificial cerebrospinal fluid (ACSF) HRI = 1.24 ± 0.74 , $n = 16,271$ motifs, 18 cells versus tetrodotoxin HRI = 0.70 ± 0.39 , $n = 1300$, 7 cells; $P < 0.01$]. Most (95.4%) motifs occurred in the absence of oscillations, as defined by whether or not a motif passed the minimum threshold for HRI when it was shifted by a putative oscillation period. The number of motifs per cell ranged from 0 to 7803, with a median of 143 motifs and HRIs ranging from 0.11 to 7.10 (mean HRI = 1.24 ± 0.74 , $n = 16,271$ motifs). The average interval between motif repetitions was 156.2 ± 113.1 s, ranging from 0.7 to 478.1 s. The average duration of a motif was 1006 ± 424 ms. In 11 out of 18 cells, motifs repeated three or more times (Fig. 1B). Although a motif could last more than 1 s and be repeated after several minutes, individual EPSCs repeated with an accuracy of better than 1 ms (Fig. 1, A and B, insets). In the 10 cells with highest HRIs, there were 4.6 ± 1.5 motifs per cell that displayed at least three postsynaptic currents (PSCs) that repeated with better than 1-ms precision. Repeating within 2-ms precision, there were 53.7 ± 22.2 motifs per cell that had at least three such precise PSCs. Finally, in simultaneously recorded neurons, repeats of intracellular motifs sometimes occurred exactly at the same time (three out of six cell pairs; 15.4 ± 3.7 simultaneous motifs per cell pair).

Repeating motifs of spontaneous synaptic activity *in vivo*. We then investigated whether repeated motifs also occurred *in vivo* using 1.5- to 10-min intracellular recordings of the spontaneous (i.e., without visual stimulation) activity from neurons in primary visual cortex of anesthetized cats (11). Repeated motifs of synaptic activity were frequent *in vivo* (19 out of 21 neurons) (Fig. 1C) and occurred mostly in the absence of oscillations (96.5%), and significantly fewer repeats were found in shuffled traces (fig. S2Cii). Many motifs detected *in vivo* consisted of very large EPSPs (>10 mV), suggestive of synchronous input from several presynaptic neurons. The mean HRI (\pm SD) was 1.30 ± 0.64 ($n = 33,374$ motifs, 19 neurons). The average duration of a repeated motif was 1035 ± 357 ms. Patterns of EPSPs lasting up to 2 s repeated with millisecond precision, even after intermotif intervals of several minutes. *In vivo* motifs also occurred more than twice (14 out of 19 neurons) (Fig. 1Cii) and could also be found to occur simultaneously in paired intracellular recordings (6 out of 9 cell pairs; 110 ± 37 simultaneous motifs per cell pair).

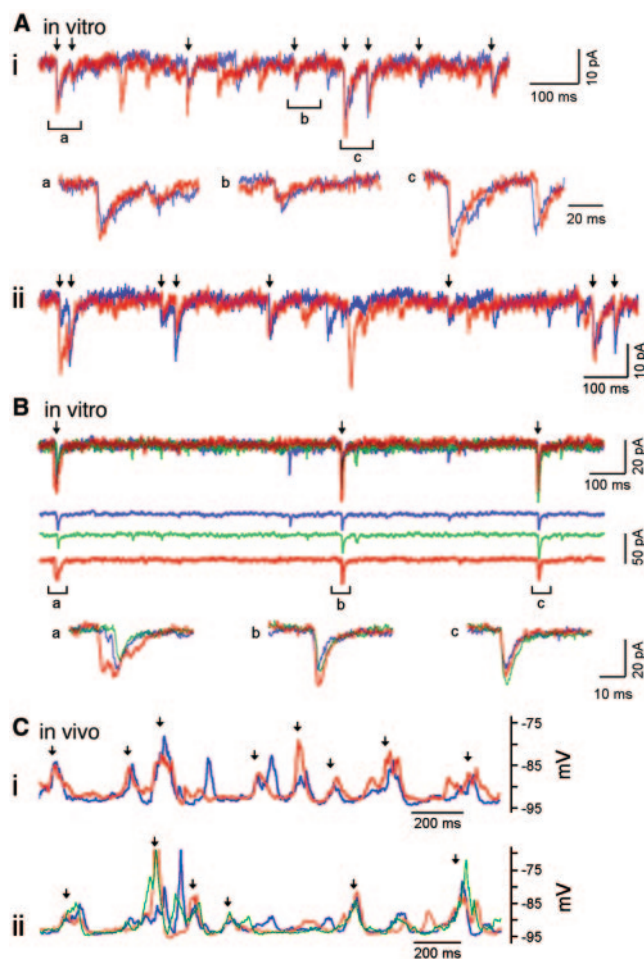
Repeated neuronal activation during motif repetition. We used calcium imaging to reconstruct, with single-cell resolution, the activity of neuronal populations (8, 12, 13)

¹Department of Biological Sciences, Columbia University, New York, NY 10027, USA. ²Department of Neurobiology and Physiology, Northwestern University, Evanston, IL 60208, USA.

*These authors contributed equally to this work.

†To whom correspondence should be addressed. E-mail: rmy5@columbia.edu

Fig. 1. Repeated motifs of spontaneous synaptic activity *in vitro* and *in vivo*. (A) Repeated motifs of intracellular activity from layer 5 pyramidal neurons in slices. Panels show segments (red) of the same voltage-clamp recording from the same cell repeating seconds or minutes after the initial occurrence (blue). Arrows indicate timings of repeated PSCs. (i) Upper trace: low-temporal resolution display of spontaneous activity of a neuron. Lower traces: higher resolution display of the repeated motif at indicated regions of the trace (a to c). (ii) Example of a longer motif. (B) Three repetitions of a motif. The top traces show the motifs superimposed on each other (blue, green, and red), the middle traces show these same traces individually, and the bottom traces show temporally magnified regions of the motifs (a to c). (C) Repeated sequences of intracellular current-clamp recordings *in vivo*. Two (i) and three (ii) repetitions of motifs are shown. Shuffle tests were performed on traces (i), a to c, yielding significantly fewer repeats (fig. S2, $P < 0.02$). In (i), the blue trace is shifted -2.75 mV; in (ii), the blue trace is shifted -1.58 mV, and the green $+0.79$ mV.



during the simultaneous occurrence of repetitions of an intracellular motif (Fig. 2). We loaded 97 brain slices from postnatal day 13 to 22 (P13 to P22) mice with calcium indicators and obtained 148 movies from primary visual and medial prefrontal cortex using confocal or two-photon microscopy. The indicator labeled virtually all superficial neurons as assessed by Nissl counterstaining (Fig. 2A). All slices displayed spontaneous calcium transients, which involved about 10% of cells during 120 s of imaging (fig. S3A). In intracellular recordings from imaged cells, spontaneous calcium transients were always synchronous with action potentials (Fig. 2B) ($n = 7$ cells) and were blocked by $1 \mu\text{M}$ tetrodotoxin or 2 mM Ni^{2+} ($n = 9$ slices). Most calcium transients were linked to action potentials generated during UP states (Fig. 2, B and C). Onset timing of action potentials could be reliably reconstructed by thresholding the first derivative of the optical traces (Fig. 2, D and E).

To explore the relation between the optically recorded sequences and the intracellular motifs, we performed intracellular recordings during slow-resolution (1 frame/s) two-photon imaging experiments. Neurons active during the first appearance of a motif were also active during its repetition (Fig. 3B) ($n = 10$ motifs; mean HRI = 1.1 ± 0.17). The mean number of optically detected neurons repeating during a motif was 3.6 ± 1.0 . The marked correlation between intracellular motifs and repeated sequences of network activity indicates that the repeated motifs are produced by the reactivation of the same circuits.

Fast imaging of spontaneous activity reveals repeating sequences. To investigate the dynamics of spontaneous activity with faster time resolution, we used confocal imaging (25 to 100 ms/frame). We created raster plots of the spontaneous activity produced by 445 to 1353 neurons (average 952.6 ± 31.3 imaged cells, $n = 57$ slices) and searched these plots with a template-matching algorithm for precisely repeating sequences of activation (7, 8). Such sequences were common, being present in 42 out of 58 movies (Fig. 3A) ($n = 3115$ sequences, average = 53.7 ± 10.3 sequences per movie, ranging from 0 to 341). Sequences involved 3 to 10 cells, lasted 2.9 ± 0.1 s (fig. S4), and repeated two to four times. To estimate the statistical significance of the occurrence of the sequences, we compared the incidence of sequences in real raster plots with surrogate raster plots obtained by three independent shuffling methods. In all types of surrogates, sequences appeared much less frequently than occurred in real data ($P \ll 0.001$) (Fig. 3, E to G). Similar results were obtained when different frames of jitter were allowed for template-matching (Fig. 3, E to

G). On average, $50.4 \pm 3.8\%$ of transients in single movies played a part in at least one sequence. For comparison, in intersignal intervals (ISI)-shuffled surrogates, at most 9.9% of transients were components of sequences. In addition, most transients simultaneously participated in different sequences; on average, individual transients were used in 1.91 ± 1.41 sequences, whereas they were used in only 0.12 ± 0.09 sequences in ISI-shuffled raster plots.

Timing and topography of repeating sequences. We further characterized the temporal and spatial structures of these repeated sequences. The timing jitter of calcium transients participating in sequences was independent of the sequence length (Fig. 3C), so the temporal precision of these sequences is preserved during their occurrence. To investigate whether these sequences persisted in time, we analyzed movies taken from the same slice for sev-

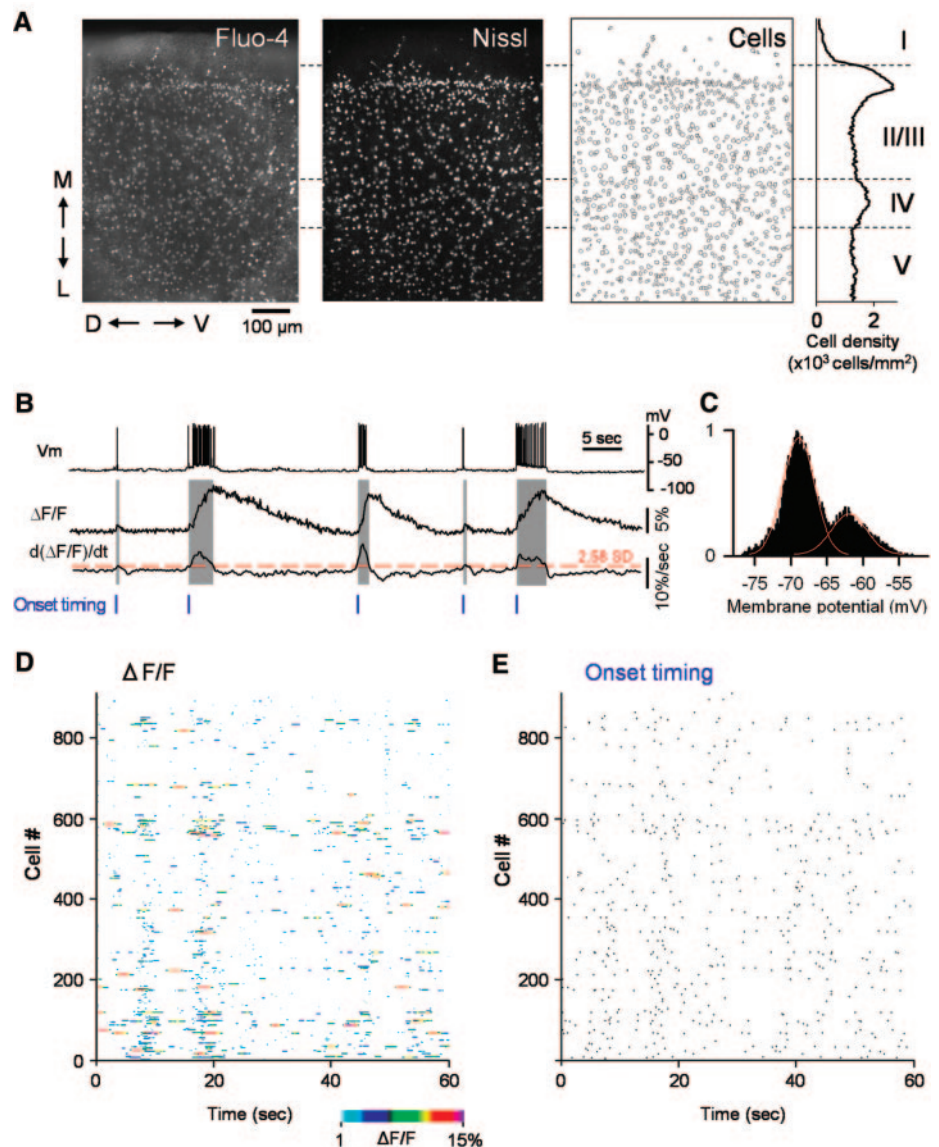


Fig. 2. Calcium imaging of spontaneous action potentials in large neuronal populations. (A) Confocal images of fluo-4 (left) and red Nissl (middle) and positions of the 866 automatically detected cells (right) of a slice of the medial prefrontal cortex. Layers were determined based on cell density. M, medial; L, lateral; D, dorsal; V, ventral. (B) Correlation between calcium transients and action potentials. Simultaneous current-clamp recording (top) and calcium imaging (middle). Onsets of spike timings (shaded areas) are detected as suprathreshold periods ($2.58 \times \text{SD}$ of noise, red) in the first derivative of the calcium signal. Most calcium transients are associated with UP states. (C) Bistable membrane potentials of a pyramidal cell. The plot was well fitted to a bimodal Gaussian distribution (red), indicative of DOWN and UP states of membrane potentials. (D) Pseudo-colored plot of calcium signals obtained from the slice in (A). Each row represents a single cell. (E) Raster-plot reconstruction of the onsets of spiking activity from (D). Out of the 866 cells, 137 cells (15.8%) showed spontaneous calcium transients.

eral hours. The subset of active cells dynamically drifted over tens of minutes (Fig. 3D and fig. S5); on average, $30.8 \pm 3.1\%$

of cells that were activated during a movie were reactivated in any subsequent movie, despite there being no prominent changes

in the total number of activated cells across movies (fig. S5A).

Sequences had specific topographic structures, in some cases involving only a particular layer or a vertical column of cells or cells located in a cluster (Fig. 4, A and B, and fig. S3B). Moreover, the spatial trajectory of the activation also precisely repeated and could follow the same direction with sequential steps. Therefore, repeating temporal patterns of activation, themselves statistically unlikely to emerge by chance, were associated with a structured spatial organization of the neurons that formed them.

Neuronal synchronization associated with the occurrence of repeated sequences.

One prediction of the “synfire” hypothesis is that repeating sequences should be specifically associated with synchronizations of the network (5). Consistent with this prediction, calcium transients were overwhelmingly produced by UP states (Fig. 2, B and C), which are reflections of circuit synchronization (13, 14). Also, time histograms of coactive cells demonstrated intermittent synchronization of spontaneous activity (Fig. 4C) (13). The synchronization appeared to be aperiodic, as assessed by Fourier analysis (fig. S6). To quantify synchronicity, we determined the *P* value of synchrony level as a function of time (Fig. 4C, red trace), defined as a probability that the same or higher level of coactivation could occur by chance in 1000 ISI-shuffled surrogates. In 52.1% of repeated sequences, the *P* value during the sequences fell below 0.05 ($n = 2983$ sequences), far in excess of what we found in ISI-shuffled data (13.6% of sequences with $P < 0.05$; $P \ll 0.001$, χ^2 test). Our analysis likely underestimates true synchronicity because we only image neurons in the plane of focus, which are a minority of the neurons present in the brain slice. Synchronization increased as a function of sequence repetition (Fig. 4D), suggesting that sequences were replayed with increasing synchrony.

Cortical songs: modular assemblies of repeated sequences.

When examining the temporal pattern of repeated sequences on larger time scales, we noticed that series of sequences could be repeated in the same sequential order (Fig. 4C). These supersequences, referred to here as “cortical songs,” were detected in 32 out of 54 movies. Each cortical song consisted of two to eight sequences (average 6.2 ± 0.1 , $n = 2636$ songs in 54 movies) and was repeated two or three times. The number of cortical songs found ranged from 0 to 321 per movie, averaging 48.8 ± 11.4 ($n = 54$ movies), far in excess of the number of songs that can emerge after shuffling of sequences (fig. S7). A sequence could par-

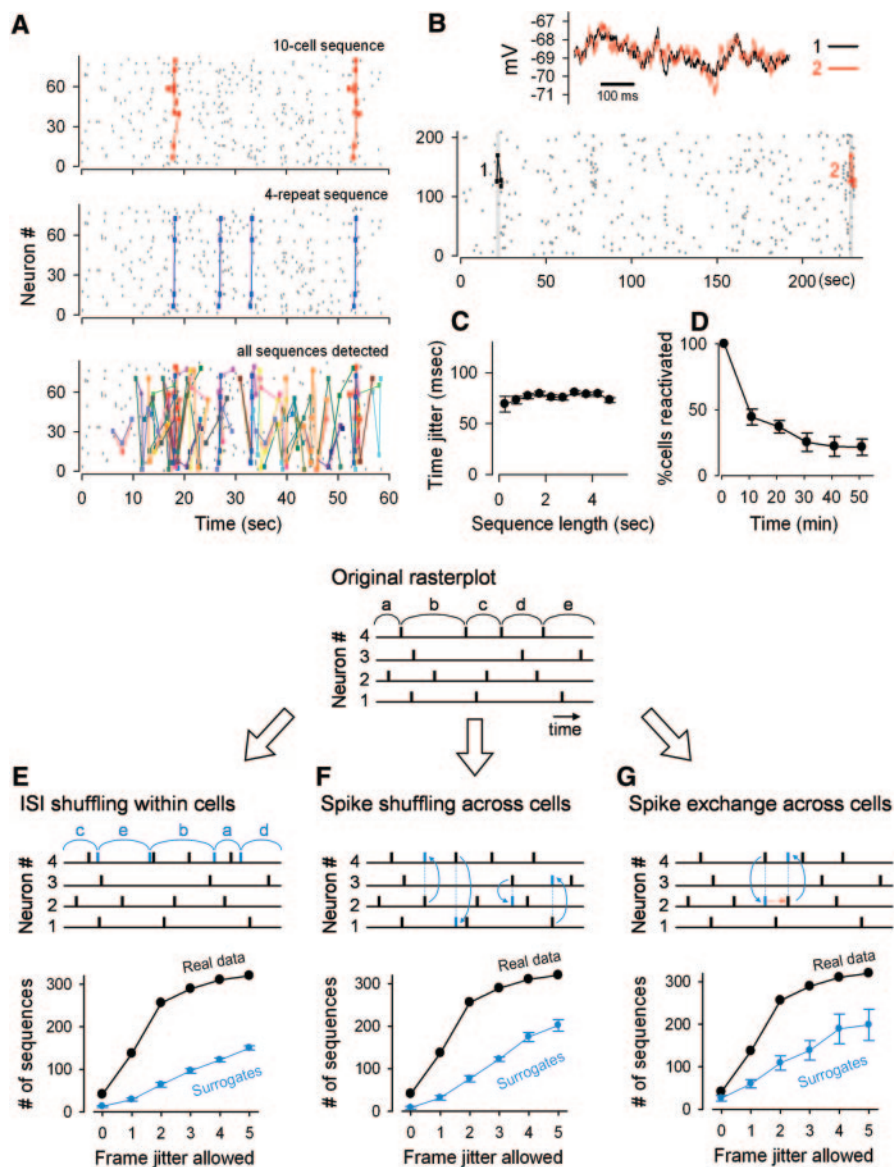


Fig. 3. Repeated motifs during sequential reactivation of identical cells. Properties of the repeated optical sequences. (A) Set of neurons with precise sequences of calcium transients (V1 slice). Ten cells (red) reactivated with exact timings between their transients (“sequence”) (top panel). In the same raster plot, a four-cell sequence (blue) is reactivated four times (middle panel). This four-cell sequence also acted as a part of the 10-cell sequence. Bottom panel shows all sequences detected in the same raster plot. (B) Simultaneous recording of intracellular motifs and repeated sequences. Raster plot displays a group of four cells activated in the same sequence during the time at which a motif and its repeat are detected simultaneously in the intracellular recording (gray, upper trace) of a layer 5 pyramidal cell. (C) The precision of the repetition is constant with the duration of the sequence. (D) Probability that cells active during a period from 0 to 2 min were reactivated in subsequent movies (means \pm SEM of six movies). (E to G) Spike sequences occur more frequently than expected by chance. Three independent methods of spike shuffling were used to examine how frequently sequences emerge by chance, as assessed by comparing the number of sequences in real spike trains (original raster plot) and their surrogates. Zero to five frames of jitter were allowed for repeated sequences. Data in Fig. 4A were analyzed (means \pm SD). (E) The intersignal intervals (ISI) were transposed at random within each cell in order to eliminate temporal correlation between the events. (F) Events were shuffled across cells while keeping their timings unchanged so as to preserve population modulation of event timings such as synchronization. (G) Spikes were exchanged between any pair of cells while maintaining their timings. The exchange procedures were repeated twice as many times as the number of spikes in the raster plot. In this randomization, event frequency within each cell and population modulation are both retained.

participate in more than one song; on average, single sequences were used in 3.7 ± 0.6 different songs ($n = 2983$ sequences). The numbers of sequences and songs detected in individual movies had a positive correlation (Fig. 4E).

The occurrence of the repeated sequences or songs was not correlated with the rate of activity (Fig. 4F), which indicates that cortical slices can generate repeated sequences, independent of the degree of network activity. In four out of six slices tested, the number of sequences and cortical songs fluctuated spontaneously without apparent changes in spike frequency.

Cortical songs were often repeated at faster time scales (Fig. 5, A and B). We quantified the temporal elasticity of the repetition with an orthogonal regression method, finding a biased distribution toward increasing compression during the course of a recording session (Fig. 5C) ($P < 0.01$) and that the precision in relative timing (as captured by the regression error) was more accurate than expected by chance (Fig. 5D). The temporal compression agrees with the increasing synchronization detected with increasing repetitions of a sequence (Fig. 4D). Also, the preservation of the precision of the songs is in accordance with the preservation of the jitter of individual sequences (Fig. 3C).

Modulation of cortical sequences and songs by NMDA and dopamine receptors.

Finally, we explored the synaptic mechanisms underlying the generation of cortical sequences and songs. It has been proposed that correlated network operation depends on *N*-methyl-D-aspartate (NMDA) receptor channel kinetics (15). In support of this proposal, the NMDA receptor antagonist APV (D,L-2-amino-5-phosphonovaleic acid) depressed the occurrence of cortical sequences and songs without affecting the activity rate (fig S8). We also compared the spatiotemporal coordination of spiking activity before and after application of dopamine, because dopamine also appears to be involved in persistent neuronal activity (16). Although we found no apparent effect of dopamine on the incidence of spiking activity, dopamine suppressed the occurrence of cortical sequences and songs (fig S9). This effect was specifically inhibited by SCH23390, a D1 receptor antagonist, and mimicked by SKF38393, a D1 agonist. Slight, but significant, increases in sequences and songs were induced by SCH23390, suggesting that endogenous dopamine is working under resting conditions. Aberrant functions of D1 receptors and NMDA receptors, both of which have been implicated in the pathophysiology of schizophrenia (17), thus induce functional disconnection of neuronal modules.

Discussion. Intracellular recordings and imaging experiments reveal the widespread existence of repeated dynamics in the spontaneous activity of neocortical circuits in vitro and in vivo. The ability to reconstruct

the activity of a large (>1000) population of neurons, and the increased statistical power of correlating intracellular records rather than spikes, have facilitated the detection of these dynamics. These repeated

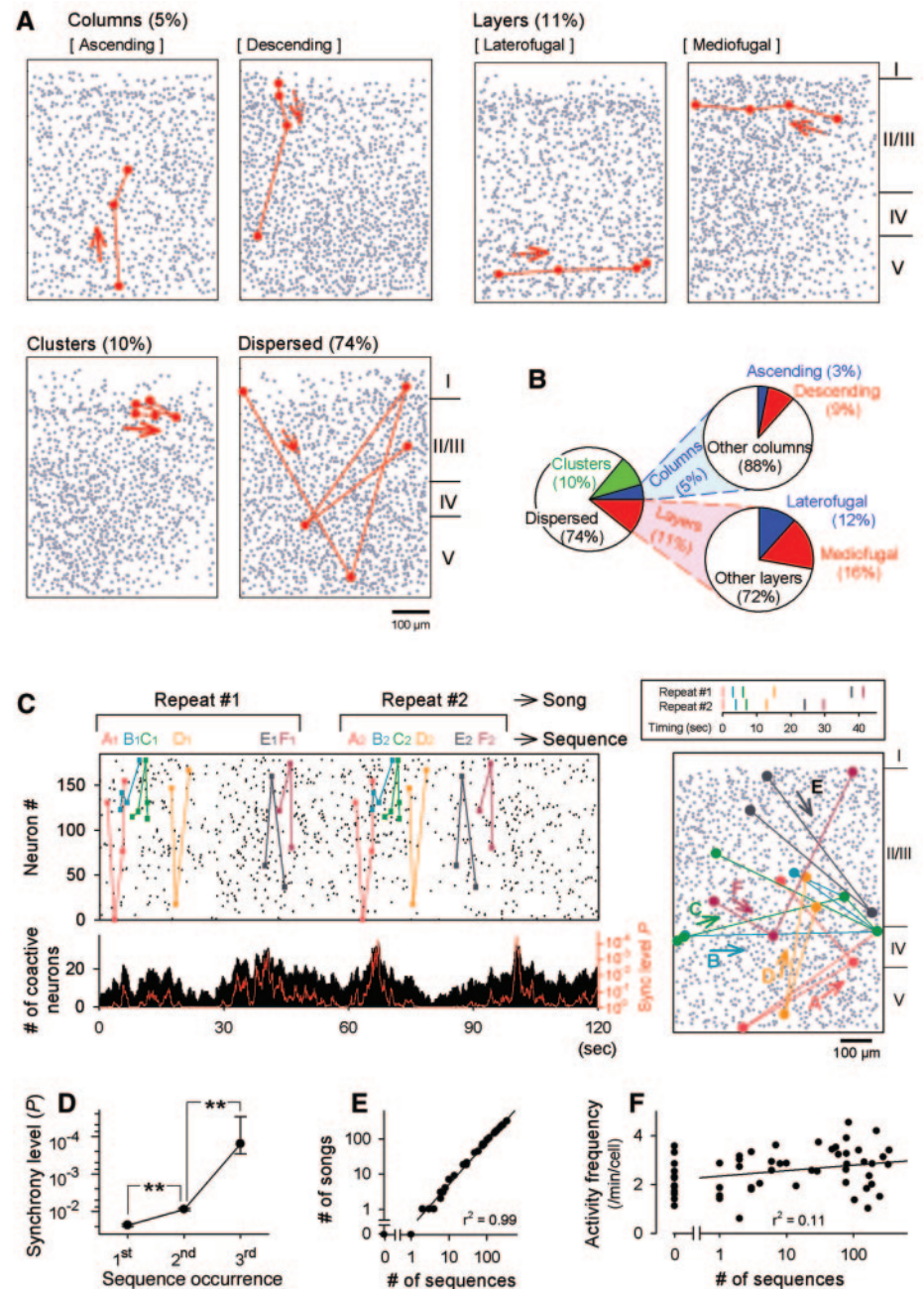


Fig. 4. Anatomical structure of the sequences. High-order sequences (cortical songs). (A) Representative maps of six types of spatial arrangement of neurons involved in sequences. Neurons are sequentially activated, as indicated by the arrows. (B) Frequency of each spatial pattern ($n = 2983$ sequences from 54 movies; medial prefrontal cortex). (C) (Left panels) Representative cortical song. A total of 181 of 1197 cells showed spontaneous activity (left top panel). Subsets of neurons displayed temporally precise sequences of activity (sequences: A1 to F2). The sequences were repeated in the same order (cortical song: A>B>C>D). Bottom histogram represents the number of cells active at each frame of the movie. The red line expresses the *P* value of synchronization, defined by random ISI shuffling (13). (Right panel) Onset timings of songs (top) and locations of cells (bottom). (D) Synchrony levels increase as a function of sequence occurrence. $**P < 0.01$; Bonferroni/Dunn test (means \pm SEM of 2983 sequences, 54 movies). (E) Correlation between the number of sequences and songs. Each dot represents a single movie. The line represents best linear fit. (F) Lack of correlation between the number of sequences and rate of activity.

patterns are robust; not only do they occur more frequently than expected by chance, but they can happen at the same time in two neurons, occur simultaneously in intracellular and optical recordings, are correlated with intracellular UP state depolarization and with network synchronizations, involve circuits with structured topographies, form modular patterns with compressing timing, and are blocked by D1 activation receptors. Our results demonstrate that the apparently stochastic cortical synapses can work with high reliability to produce stereotypical dynamics that are reduced in dimensional space. Our data agree with the prediction that cortical activity flows through chains of synchronized neurons (synfire chains), which are reactivated with high temporal precision. Moreover, we describe a higher order grammar (18), by which these chains themselves can be modules of larger tem-

poral structures (cortical songs), defined by their sequential order of activation, and which can last for minutes. These songs resemble spiking correlates of sequential behavior, like bird songs (19, 20) or spatial navigation (21), and have compressing dynamics, as if the circuit was replaying and modifying previously learned sequences (21–23). The mechanisms that generate and propagate synfire chains and cortical songs must be intrinsic to the cortical circuit, because they are preserved in slices, and might reflect the faithful reactivation of specific circuits (24), mediated by stereotypical synaptic dynamics (25, 26) and driven by pacemaker cells (8, 27). Because the activity drifts with time, it is also possible that short-lived patterns, perhaps reflecting ongoing circuit memory, are generated de novo (6, 28). Regardless of the mechanism, the repeated dynamics that we

observed involve UP states, and the progression of activity is therefore briefly settling into preferred states of persistent activity, so our data link synfire chains with attractor neural networks (6, 13, 29). We conclude that the neocortex can spontaneously generate precisely reverberating temporal patterns of activation (5, 30), dynamic ensembles that could represent endogenous building blocks of cortical function (31, 32).

References and Notes

1. V. B. Mountcastle, *Perceptual Neuroscience: The Cerebral Cortex* (Harvard Univ. Press, Cambridge, MA, 1998).
2. H. Markram, M. Tsodyks, *Nature* **382**, 807 (1996).
3. L. F. Abbott et al., *Science* **275**, 220 (1997).
4. C. Stevens, *Curr. Biol.* **4**, 268 (1994).
5. M. Abeles, *Corticonics* (Cambridge Univ. Press, Cambridge, 1991).
6. M. Diesmann, M. O. Gewaltig, A. Aertsen, *Nature* **402**, 529 (1999).
7. M. Abeles et al., *J. Neurophysiol.* **70**, 1629 (1993).
8. B. Q. Mao et al., *Neuron* **32**, 883 (2001).
9. M. W. Oram et al., *J. Neurophysiol.* **81**, 3021 (1999).
10. Materials and methods are available as supporting material on Science Online.
11. I. Lampl, I. Reichova, D. Ferster, *Neuron* **22**, 361 (1999).
12. R. Yuste, L. C. Katz, *Neuron* **6**, 333 (1991).
13. R. Cossart, D. Aronov, R. Yuste, *Nature* **423**, 283 (2003).
14. Y. Shu, A. Hasenstaub, D. A. McCormick, *Nature* **423**, 288 (2003).
15. X. J. Wang, *Trends Neurosci.* **24**, 455 (2001).
16. P. S. Goldman-Rakic, *Neuron* **14**, 477 (1995).
17. W. Franke, J. Lerma, M. Laruelle, *Neuron* **39**, 205 (2003).
18. E. Bienenstock, *Neural Comput.* **6**, 179 (1995).
19. F. Nottebohm et al., *Philos. Trans. R. Soc. London B Biol. Sci.* **329**, 115 (1990).
20. R. H. Hahnloser, A. A. Kozhevnikov, M. S. Fee, *Nature* **419**, 65 (2002).
21. K. Louie, M. Wilson, *Neuron* **29**, 145 (2001).
22. W. L. Skaggs, B. L. McNaughton, *Science* **271**, 1870 (1996).
23. Z. Nadasdy, H. Hirase, A. Czurko, J. Csicsvari, G. Buzsaki, *J. Neurosci.* **19**, 9497 (1999).
24. J. Kozloski, F. Hamzei-Sichani, R. Yuste, *Science* **293**, 868 (2001).
25. G. Silberberg, C. Wu, H. Markram, *J. Physiol.* **556**, 19 (2004).
26. D. V. Buonomano, *Proc. Natl. Acad. Sci. U.S.A.* **100**, 4897 (2003).
27. R. R. Llinás, *Science* **242**, 1654 (1988).
28. W. Maass, T. Natschlagler, H. Markram, *Neural Comput.* **14**, 2531 (2003).
29. J. J. Hopfield, *Proc. Natl. Acad. Sci. U.S.A.* **79**, 2554 (1982).
30. R. Lorente de Nó, *J. Neurophysiol.* **1**, 207 (1938).
31. A. Grinvald et al., *Biopolymers* **68**, 422 (2003).
32. R. Llinás, *I of the Vortex: From Neurons to Self* (MIT Press, Cambridge, MA, 2002).
33. We thank D. Anastassiou for access to the Regatta supercomputer, W. Maass and members of our laboratory for comments, and the late P. Goldman-Rakic for suggestions and encouragement. Supported by the National Eye Institute, National Institute of Neurological Disorders and Stroke, University of Tokyo, and the New York State Office of Science, Technology and Academic Research (NYSTAR).

Supporting Online Material

www.sciencemag.org/cgi/content/full/304/5670/559/DC1

Materials and Methods

Figs. S1 to S9

References

Movies S1 and S2

31 October 2003; accepted 18 February 2004

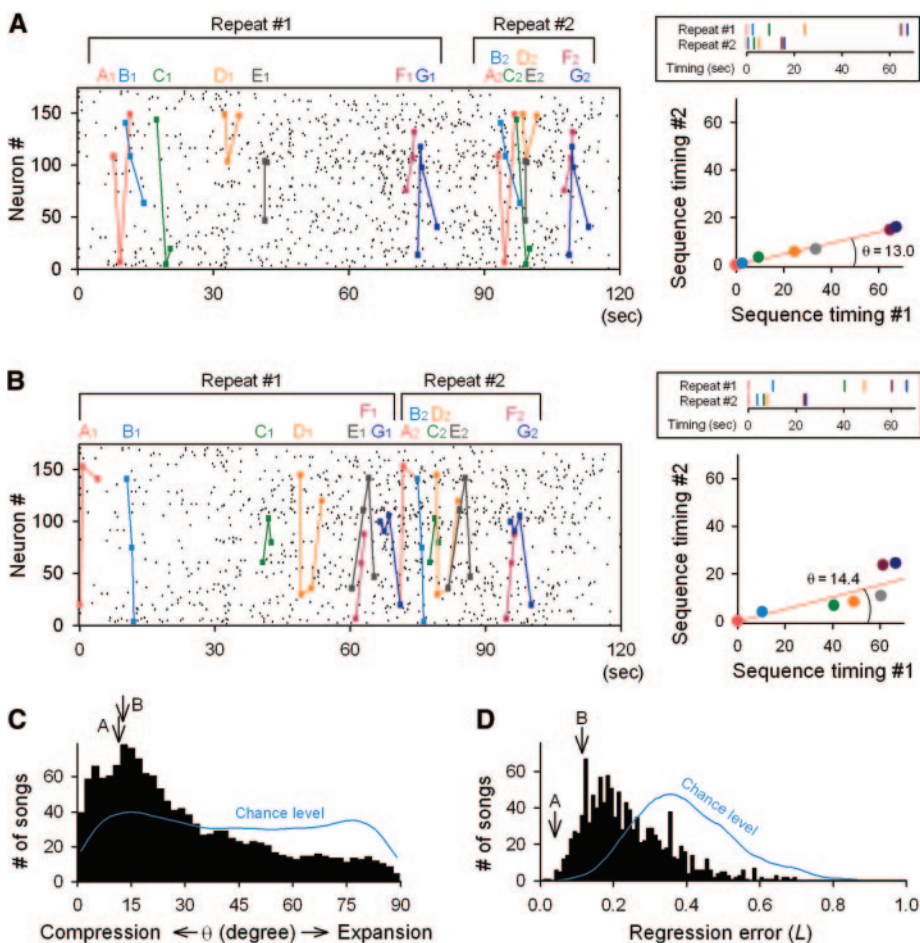


Fig. 5. Temporal compression of cortical songs. (A and B) Representative songs repeating at faster time scales, both found in the same raster plot. Right top panel indicates the onset timings of the sequences in each song. The right bottom scatter plots show regression analyses for timing correlations of the first song occurrence versus the second recurrence. (C) Asymmetric distribution of θ (average = $29.2^\circ \pm 0.6^\circ$; mean \pm SEM of 2636 songs, 54 movies). The distribution of 22,824 surrogate songs obtained for shuffled sequences (fig. S7) is shown as a chance level (blue). The values of the songs shown in the (A) and (B) are indicated by the arrows. (D) The distribution of regression error (L) after the pseudo-rotation coordinate transformation (10). The mean L values in the real data were significantly lower than expected by chance ($P < 0.001$; Bonferroni/Dunn test).